Characteristics of Langmuir electric field waveforms and power spectra exhibiting nonlinear behavior in Earth's foreshock

K. Sigsbee,[1] C. A. Kletzing,[1] J. S. Pickett,[1] D. A. Gurnett,[1] S. J. Schwartz,[2] B. Lefebvre,[3] E. Lucek,[2] A. N. Fazakerley,[4] and H. Kucharek[3]

Received 30 September 2009; revised 28 June 2010; accepted 7 July 2010; published 29 October 2010.

[1] Langmuir wave characteristics in the Earth's foreshock were examined to identify possible nonlinear wave behavior for two case studies with data from the Cluster Wideband Data Plasma Wave Receiver. The occurrence rates of four types of power spectra near the foreshock edge were determined: (1) spectra with power at the local plasma frequency f_{pe} only, (2) spectra with power at f_{pe} and $2f_{pe}$, (3) spectra with double peaks near f_{pe}, and (4) spectra with double peaks near f_{pe} and peaks at low frequencies indicative of ion acoustic waves. For electric field waveform amplitudes between 0.1 and 22.0 mV/m, most power spectra fell into the f_{pe} only and double-peaked categories. The maximum Langmuir wave amplitudes and bump-on-tail reduced electron distribution functions from Cluster PEACE data were more consistent with saturation of wave growth by electrostatic decay than modulational instabilities. However, few spectra had the double peaks near f_{pe} and ion acoustic waves indicative of electrostatic decay, suggesting other processes may also be at work. For amplitudes greater than 22.0 mV/m, most power spectra fell into the f_{pe} and $2f_{pe}$ category, but many of the harmonics were too weak to be clearly distinguished from harmonics caused by instrumental effects.

Citation: Sigsbee, K., C. A. Kletzing, J. S. Pickett, D. A. Gurnett, S. J. Schwartz, B. Lefebvre, E. Lucek, A. N. Fazakerley, and H. Kucharek (2010), Characteristics of Langmuir electric field waveforms and power spectra exhibiting nonlinear behavior in Earth's foreshock, *J. Geophys. Res.*, *115*, A10251, doi:10.1029/2009JA014948.

1. Introduction

[2] Just upstream from the Earth's bow shock, the foreshock region is connected to the bow shock by the interplanetary magnetic field and populated by solar wind particles accelerated and reflected at the bow shock by a fast Fermi process [*Leroy and Mangeney*, 1984; *Wu*, 1984]. *Filbert and Kellogg* [1979] were the first to suggest that the Langmuir waves (~3–30 kHz) observed in the foreshock [*Scarf et al.*, 1971; *Fredricks et al.*, 1971] were related to beam-like electrons reflected and accelerated at the quasi-perpendicular bow shock near the point where the interplanetary magnetic field is tangent to the bow shock.

[3] Many observations have been made of linear and nonlinear Langmuir wave behavior and unstable electron populations in the Earth's foreshock. Observations have been made of impulsive, broadband electrostatic waves at frequencies well above or below the local plasma frequency f_{pe} [*Lacombe et al.*, 1985], which are often referred to as downshifted plasma oscillations [*Fuselier et al.*, 1985], and explained in terms of electron acoustic waves driven unstable by ion and electron beams [*Marsch*, 1985]. However, the focus of this paper is on waves at harmonics of the plasma frequency [*Gurnett*, 1975], which have been observed by many spacecraft since the 1970s, and the nonlinear processes which may generate these waves. Data from ISEE-1 and ISEE-3 [*Hoang et al.*, 1981; *Lacombe et al.*, 1988] and Geotail [*Kasaba et al.*, 1997; 2000] showed that the source region of the $2f_{pe}$ radio emissions is the electron foreshock, the leading edge of the foreshock where the largest amplitude Langmuir waves are found, and that the intensity of the $2f_{pe}$ emissions generally depends upon the intensity of the Langmuir waves. Although these waves are thought of as harmonics, the frequency of the waves is not always twice the local value of f_{pe}. Bifurcations of the emissions near $2f_{pe}$ have been observed by ISEE-3 and Geotail and are thought to be caused by solar wind density discontinuities passing the satellite [*Lacombe et al.*, 1988; *Kasaba et al.*, 1997]. Other observations have suggested that waves at higher order harmonics of f_{pe} may also be observed [*Cairns*, 1986].

[4] Evidence has been found for nonlinear three-wave interactions in the Earth's foreshock [*Bale et al.*, 1996; *Kellogg et al.*, 1996; *Walker et al.*, 2003], which may explain the generation of these waves at harmonics of the plasma frequency [*Cairns and Melrose*, 1985] and the modulations of the Langmuir wave envelopes [*Cairns and*

[1]Department of Physics and Astronomy, University of Iowa, Iowa City, Iowa, USA.
[2]Space and Atmospheric Physics Group, The Blackett Laboratory, Imperial College, London, United Kingdom.
[3]University of New Hampshire, Space Science Center, Durham, New Hampshire, USA.
[4]Mullard Space Science Laboratory, Dorking, United Kingdom.

0148-0227/10/2009JA014948

Robinson, 1992]. In these theories, beam-driven Langmuir waves undergo a decay or a coalescence with preexisting ion acoustic waves, generating a secondary spectrum of backscattered Langmuir waves,

$$L \pm S \rightarrow L', \tag{1}$$

where L is a beam-driven Langmuir wave, S is an ion acoustic wave, and L' is a backscattered Langmuir wave. Harmonics can be generated if the backscattered waves and beam-driven waves coalesce to produce transverse electromagnetic waves at roughly twice the local plasma frequency $2f_{pe}$,

$$L + L' \rightarrow T, \tag{2}$$

where L and L' are the beam-driven and backscattered Langmuir waves as before, and T is a transverse electromagnetic wave. Wind spacecraft observations included a variety of different waveforms and power spectra in the Earth's foreshock, with examples of possible three-wave interactions in the form of power spectra with peaks at two separate frequencies near the plasma frequency [*Kellogg et al.*, 1996]. The difference in frequency between the two peaks was consistent with an ion acoustic wave. Bicoherence analysis performed on Wind waveforms [*Bale et al.*, 1996] and Cluster Wideband Data (WBD) Plasma Wave Receiver electric field waveforms [*Walker et al.*, 2003] also showed evidence for nonlinear three-wave interactions in the Earth's foreshock. Bicoherence and wavelet analysis of STEREO S/WAVES data shows that three-wave interactions may also occur during type III emissions [*Henri et al.*, 2009]. Results from Cluster have shown that Langmuir waves in the foreshock could also undergo parametric decay into an electron acoustic wave and an ion acoustic wave [*Soucek et al.*, 2005], instead of the interaction shown in equation (1).

[5] For two case studies, we have examined the occurrence rates of four different types of electric field power spectra observed by Cluster near the foreshock's boundary with the solar wind in order to gauge the importance of nonlinear interactions and to experimentally determine the electrostatic decay threshold. The types of power spectra considered were: (1) spectra with power at f_{pe} only, (2) spectra with power at f_{pe} and $2f_{pe}$, (3) spectra with double peaks near f_{pe} but no low frequency waves, and (4) spectra with double peaks near f_{pe} accompanied by low frequency waves identified as ion acoustic waves. Type (2) provides evidence for the nonlinear interaction described in equation (2) that is thought to produce waves at harmonics of the plasma frequency [e.g., *Cairns and Melrose*, 1985; *Cairns*, 1986]. Types (3) and (4) provide evidence for the nonlinear interaction described in equation (1), which may supply the backscattered Langmuir waves required for the interaction described in equation (2) [e.g., *Bale et al.*, 1996; *Walker et al.*, 2003]. We did not consider downshifted waves or beam mode waves [*Etcheto and Faucheux*, 1984; *Lacombe et al.*, 1985; *Marsch*, 1985] in this paper. In our study, we classified waves as downshifted if their power spectra featured a single, broad peak more than 10 kHz wide near the plasma frequency. Although examples of downshifted waves were found near the foreshock edge in both case studies, these waves are more typically found deep within the foreshock, not near the edge. Downshifted waves may be produced by beams with speeds on the order of the electron thermal speed [*Fuselier et al.*, 1985] or a loss-cone instability [*Lobzin et al.*, 2005], rather than the more energetic electron beams found near the boundary between the foreshock and solar wind. This paper will instead concentrate on evidence for the nonlinear interactions involved in generating double-peaked power spectra and $2f_{pe}$ emissions near the foreshock edge, where the largest amplitude waves and most energetic electron beams are found. We will also discuss nonlinear instrumental behavior that may obscure the actual behavior of waves in the foreshock.

2. Foreshock Data Sets

[6] In the 77 kHz bandwidth mode, the Cluster WBD Plasma Wave Receiver [*Gurnett et al.*, 1997] obtains two back-to-back ~5 ms electric field waveforms every 79.5 ms. The gain of the WBD receiver is set over a range of 75 dB in 5 dB increments. In the automatic gain control (AGC) mode, the gain state is adjusted to keep the measured average signal within the range of the digitizer. The full peak amplitude range of the WBD Plasma Wave Receiver is approximately 2.6×10^{-5} mV/m to 36.9 mV/m or 123 dB. The waveforms are digitized using a linear, 8-bit analog-to-digital converter and the dynamic range in each gain state covers 48 dB within the full 123 dB range. As a result of the 8-bit digitization, the uncalibrated WBD waveform electric fields have integer byte values ranging between 0 and 255 counts. To calculate the power spectra used in this paper, we applied a Hanning window to each 5 ms waveform and then performed a Fast Fourier Transform (FFT).

[7] Langmuir wave amplitudes in the Earth's foreshock can change on time scales less than 1 ms, so the 0.1 s cadence at which the gain is updated in AGC mode can result in occasional clipping of the waveform peaks when the amplitudes exceed the range of the current gain setting. The power spectra of clipped waveforms often exhibit significant power at odd harmonics of the plasma frequency, while the even harmonics feature relatively low power. These harmonics are a purely instrumental effect [*Walker et al.*, 2002] so clipped waveforms were not used in our study.

[8] The WBD receiver amplifiers can also introduce instrumental harmonics for a sine wave test input even when the output waveforms are not clipped. These harmonics arise due to small nonlinearities in the receiver amplifiers which can generate harmonics at very low levels for strong input signals. This type of nonlinear behavior is a feature of all amplifier circuits and is not unique to the amplifiers used in the Cluster WBD Plasma Wave Receiver. Nonlinear behavior in the WBD receiver amplifiers has previously been explored by *Walker et al.* [2002] for a variety of input signals. For our study, we have performed extensive bench tests on a spare, flight-quality WBD receiver to investigate these sources of instrumental harmonics and measure the power levels of these harmonics relative to the input sine wave power. The results of these tests and their implications for foreshock studies will be discussed in Section 4 of this paper.

[9] Converting analog field measurements into digital waveforms may introduce nonphysical peaks into the power spectra of the waveforms recorded by the Cluster WBD Plasma Wave Receiver and other similar instruments. For example, the Wind WAVES Time Domain Sampler (TDS) [*Bougeret et al.*, 1995] was designed as an 8-bit analog-to-log-digital waveform receiver and optimized for recording intense, bursty signals with large amplitude variations. Although waves at harmonics of f_{pe} were observed by the Wind WAVES TDS near collisionless shocks, *Kellogg* [2003] was reluctant to claim these harmonics were real because the TDS data were compressed using a logarithmic converter, which could have introduced instrumental artifacts into the data. In a study of Type II emissions from interplanetary shocks, *Farrell et al.* [2004] documented the effects of the logarithmic converter on power spectra. They showed that the nonlinear Wind WAVES TDS signal digitization does indeed introduce sampling noise related spikes into the spectra, so that caution was needed in data interpretation.

[10] To investigate possible signal digitization effects on the power spectra of Cluster WBD waveforms, we used a computer program to create a series of test waveforms and simulate the signal digitization. The test waveforms consisted of combinations of sine waves at various frequencies and amplitudes that simulated Langmuir waves at the plasma frequency, waves at the plasma frequency and twice the plasma frequency, waves with a double peak near the plasma frequency, waves with a double peak near the plasma frequency and ion acoustic waves, and strong ion acoustic waves with very weak Langmuir waves. We simulated waveforms whose power spectra featured narrow peaks at a fixed frequency and waveforms whose power spectra featured broad peaks and frequencies that varied linearly with time. Exponentially decaying envelopes were also used in some test signals. The same waveform capture length and sampling rate as the 77 kHz mode employed in space-based measurements made by the WBD receiver were used in each test signal. The test waveforms were created assuming typical foreshock amplitudes in mV/m and various gain settings, then rescaled into arrays of continuous floating point values between 0.0 and 255.0 using the WBD calibration parameters. To simulate digitization effects, the test waveforms were converted to integer byte values by dropping the decimal portion of each floating point value. We applied a Hanning window and performed the FFT on each waveform. Then we compared the power spectra of waveforms scaled between floating point values of 0.0 and 255.0 with the power spectra of digitized waveforms with integer values between 0 and 255 counts. The main effect of the signal digitization is to raise the noise floor of the power spectra. The linear signal digitization scheme used by the WBD Plasma Wave Receiver does not appear to introduce harmonics or other artifacts into power spectra as long as the waveforms are well ranged for the gain setting used, unlike the logarithmic signal digitization used by the Wind WAVES TDS. However, it is possible that the WBD Plasma Wave Receiver digitization still has some influence for small amplitude waves. Guided by these results, we decided to ignore waveforms with peak amplitudes in the lowest 10.5 dB of the 48 dB range for each gain state, as their amplitudes fell below the digitization threshold at which a clear signal can be determined. These steps ensured that the waveforms and spectra used were well defined.

[11] Because the WBD receiver antenna is located in the spin plane of the Cluster spacecraft, measurements near the plasma frequency in the foreshock can exhibit an amplitude modulation with a period of half the spacecraft spin period (4 s) due to the changing antenna orientation with respect to the background magnetic field. This spin modulation can be used to confirm that the waves are consistent with Langmuir waves, and not upper hybrid waves, which have a frequency given by

$$f_{UH} = \sqrt{f_{pe}^2 + f_{ce}^2}, \tag{3}$$

where f_{pe} is the plasma frequency and f_{ce} is the electron cyclotron frequency. Because of the small magnetic fields in the solar wind, the cyclotron frequency in the foreshock may only be a few hundred Hz. As a result, the upper hybrid frequency can be quite close to the plasma frequency. For Langmuir waves, the wave vector **k** is parallel to the background magnetic field, but the wave vector for upper hybrid waves is perpendicular to the background magnetic field. Although the electric field amplitudes do not completely go to zero when the antenna is oriented perpendicular to the magnetic field, the spin modulation patterns are more consistent with Langmuir waves than upper hybrid waves. The maximum electric field amplitudes are generally observed when the angle between the antenna and the background magnetic field is the smallest, and the minimum electric field amplitudes are found when this angle is close to 90°. Similar patterns of amplitude variation with the antenna orientation relative to the magnetic field were observed on wind [*Bale et al.*, 2000]. Detailed analysis by *Bale et al.* indicated that the foreshock wave amplitude distributions were peaked at 0° and 180° relative to the magnetic field.

[12] To obtain a more accurate measure of the Langmuir wave electric field amplitudes, the waveform amplitudes can be corrected to their assumed full amplitude along the background magnetic field [e.g., *Sigsbee et al.*, 2004a, 2004b; *Soucek et al.*, 2005]. This requires that the measured electric fields be multiplied by a correction factor of $1.0/\cos\theta$, where θ is the angle between the antenna and the magnetic field. When we applied the spin modulation correction, data taken from $79° \leq \theta \leq 101°$ were rejected because the amplitude correction factor becomes very large for angles close to 90°. Rejecting waveforms observed near 90° relative to the background magnetic field also helps ensure that we are only including Langmuir waves and not upper hybrid waves. Applying the antenna angle correction to the waveform amplitudes increases the maximum peak amplitude that can be measured from 36.9 mV/m to 184.5 mV/m.

[13] We used magnetic field and solar wind data from ACE, along with magnetic field data from the Cluster FGM experiment [*Balogh et al.*, 2001] to determine Cluster's location relative to the foreshock boundary. Cluster PEACE data [*Johnstone et al.*, 1997] and CIS data [*Reme et al.*, 2001] were used to aid in calculations of the threshold for

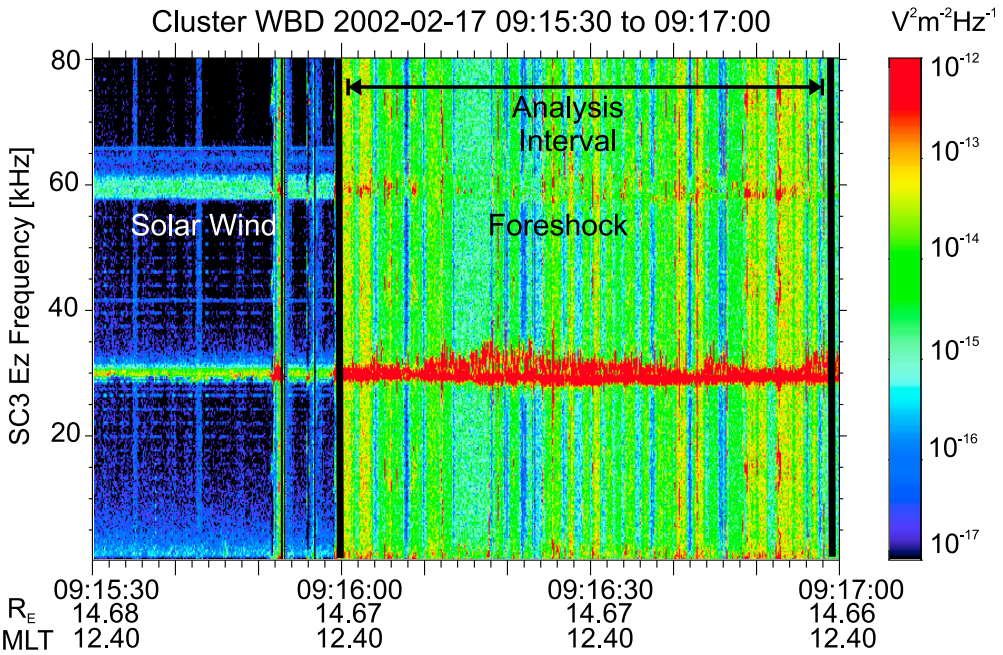

Figure 1. Spectrogram showing the Langmuir waves observed by Cluster spacecraft 3 in the foreshock on 17 February 2002. The marked analysis interval is the time period considered in Figures 4 and 6.

the three-wave decay thought to explain the double-peaked power spectra.

3. Case Studies

[14] The intent of this study is to determine the occurrence rates and properties of different types of power spectra observed in the foreshock during short intervals of Cluster data from 17 February 2002 and 21 January 2002. We selected these time periods because they featured similar solar wind conditions and wave amplitudes. Cluster was also located at approximately the same distance from the boundary between the foreshock and the solar wind and the same distance from the point at which the solar wind magnetic field is tangent to the bow shock for the time periods considered, based upon the standard foreshock coordinate system [*Filbert and Kellogg*, 1979; *Cairns et al.*, 1997].

[15] On 17 February 2002, Cluster was located mainly inside the foreshock from 09:13:00–10:13:00 UT, except for a brief entry into the solar wind from 09:13:35–09:15:59 UT due to solar wind magnetic field variations. Throughout this time period, the plasma frequency remained steady near 30 kHz, as shown in Figure 1. We considered the types of power spectra found just after the spacecraft left the solar wind and reentered the foreshock, between 09:15:59–09:16:59 UT. During this short interval, Cluster was located near 12.4 MLT, within 1 R_E of the foreshock boundary and about 5 R_E from the magnetic tangent point using the standard foreshock coordinate system [*Filbert and Kellogg*, 1979; *Cairns et al.*, 1997] determined from the Cluster FGM data, ACE solar wind parameters, and a paraboloid bow shock model [*Sigsbee et al.*, 2004a, 2004b]. For the time period studied, solar wind conditions were steady and close to average values, with V_{SW} ~420 km/s, n_{sw} ~11 cm^{-3}, and a dynamic pressure of ~3 nPa. The maximum uncorrected electric field amplitude measured by the Cluster WBD receiver on spacecraft 3 without clipping from 09:15:59–09:16:59 UT was 34.0 mV/m, and the average of the uncorrected peak electric field amplitudes for each waveform capture in this interval was 3.1 mV/m. When corrected for spin modulation effects due to the WBD antenna orientation relative to the magnetic field, the maximum amplitude during this time period was 69.7 mV/m and the average amplitude was 5.8 mV/m. The time period studied here included some of the data from the narrow region of high wave amplitudes near the foreshock edge shown in Figure 2 of *Sigsbee et al.* [2004a].

[16] On 21 January 2002, Cluster moved in and out of the foreshock, solar wind, and magnetosheath between 01:15–03:45 UT. Although the magnetic field was not steady on this day, the solar wind conditions were similar to those on 17 February 2002, with V_{SW} ~440 km/s, n_{sw} ~10 cm^{-3}, and a dynamic pressure of ~3 nPa. During this time period, Cluster was located near 14.2 MLT, within 1 R_E of the foreshock boundary and 5–7 R_E from the magnetic tangent point. For this study, we selected the interval 01:54:20–01:54:44 UT, just after Cluster left the solar wind and entered the foreshock, as shown in Figure 2. Although Cluster crossed the boundary between the foreshock and the solar wind several times on this day, we focused on data from 01:54:20–01:54:44 UT because of the large amplitude waves observed during this interval. During this time period, the maximum uncorrected electric field amplitude measured by the Cluster WBD receiver on spacecraft 4 was 35.5 mV/m, and the average of the uncorrected peak electric field amplitudes for each waveform capture in this interval was 3.8 mV/m. When corrected for spin modulation effects, the maximum amplitude during this time interval increased to 82.3 mV/m and the average amplitude increased to

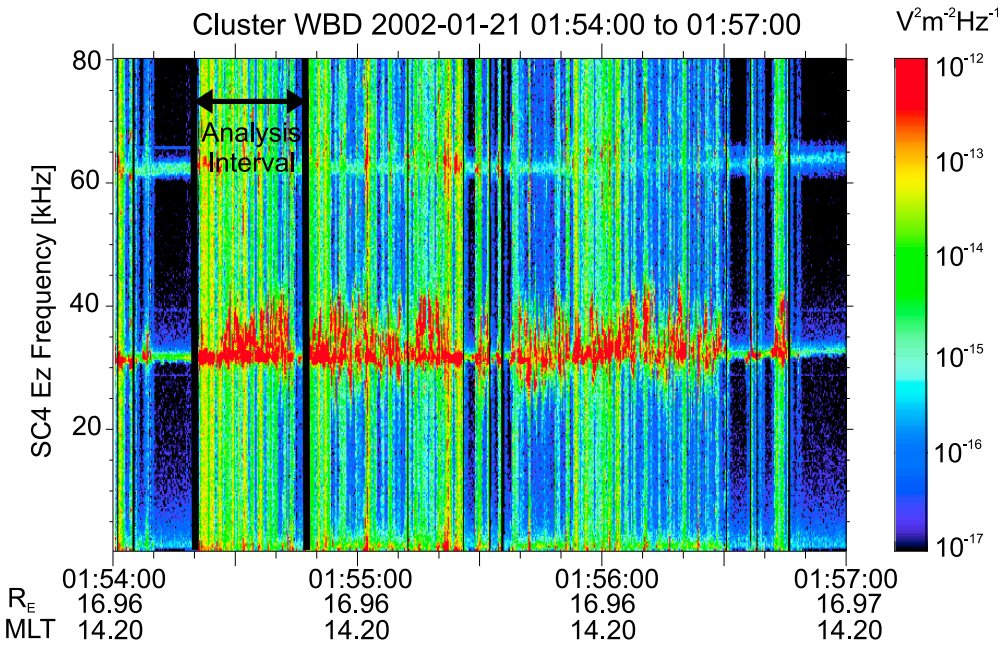

Figure 2. Spectrogram showing the Langmuir waves observed by Cluster spacecraft 4 in the foreshock on 21 January 2002. The marked analysis interval is the time period considered in Figures 4 and 6.

7.5 mV/m. These amplitudes are comparable to the amplitudes observed on 17 February 2002, in spite of the more variable solar wind conditions.

[17] Examples of waveforms and power spectra from the two case study time periods illustrating the four power spectra categories we considered are shown in Figure 3. The amplitudes of these waveforms and their power spectra have not been corrected for the spacecraft spin modulation. Panel 3(a) shows an example waveform and the corresponding spectrum with power at f_{pe} only, 3(b) with power at f_{pe} and $2f_{pe}$, 3(c) with double peaks near f_{pe} but no low frequency waves, and 3(d) with double peaks near f_{pe} and a low frequency peak that represents ion acoustic waves. Power spectra that are characterized only by a peak at f_{pe} often have very narrow peaks, as shown in Figure 3(a), but the width of this peak is variable and downshifted waves with broad peaks can look similar. To eliminate the possibility of mixing the single peak data with that of downshifted waves, we did not consider power spectra that had a single peak near f_{pe} more than 10 kHz wide.

[18] Power spectra, such as the example in Figure 3(b) with peaks at f_{pe} and $2f_{pe}$, suggest that nonlinear three-wave interactions have taken place, according to theories of harmonic generation. Power spectra such as the examples shown in Figures 3(c) and 3(d) featuring double peaks near the local plasma frequency provide evidence for the beam-driven and backscattered Langmuir wave populations described in theories of nonlinear three-wave interactions. However, only the example shown in Figure 3(d) provides evidence of all three types of waves involved in these interactions: the beam-driven Langmuir waves, backscattered Langmuir waves, and the lower frequency ion acoustic waves. Similar power spectra would also result from the decay of Langmuir waves into electron acoustic waves and ion acoustic waves [*Soucek et al.*, 2005]. The waveform in Figure 3(c) has a gentle envelope modulation, while the waveform corresponding to the double-peaked power spectra in Figure 3(d) shows evidence for beating between the two Langmuir wave populations in the form of phase changes near the zero crossings of the waveform envelope. The waves near $2f_{pe}$ also show a double-peaked structure in Figure 3(d). The waveform corresponding to the spectrum shown in Figure 3(d) was well ranged for the gain state in which this waveform was recorded, so this waveform was not clipped nor does it appear to be affected by the signal digitization. The double-peaked harmonic in Figure 3(d) also does not exactly fit the profile of previously documented WBD instrumental effects associated with beating waveforms [*Walker et al.*, 2002]. However, it still appears likely that the harmonics shown in Figure 3(b) and 3(d) are related to the response of the WBD receiver amplifiers. This will be discussed in more detail in Section 4.

[19] To understand the significance of nonlinear processes in the foreshock, we examined the occurrence rates of the four types of Langmuir wave power spectra. Clipped waveforms and waveforms with peak electric field values below a minimum threshold were not included in this analysis. We also considered only waveforms with power spectra that have the largest peak above 4 kHz to eliminate cases where ion acoustic waves were the dominant mode. On 21 January 2002, the average frequency of the peak near f_{pe} was around 26.8 kHz, but the location of the peak was highly variable and sometimes reached values near 40 kHz. Because of this variability in f_{pe}, waveforms where the expected harmonic was above 77 kHz were eliminated as they are above the filter cutoff for this operating mode. Waveforms for which the expected $2f_{pe}$ peak in the power spectra was between 64.5 and 67.0 kHz were not included in order to avoid the interference line at 65.75 kHz produced by the spacecraft battery subsystem. Each foreshock waveform was placed into only one category. The double peak and double peak with ion acoustic waves categories were

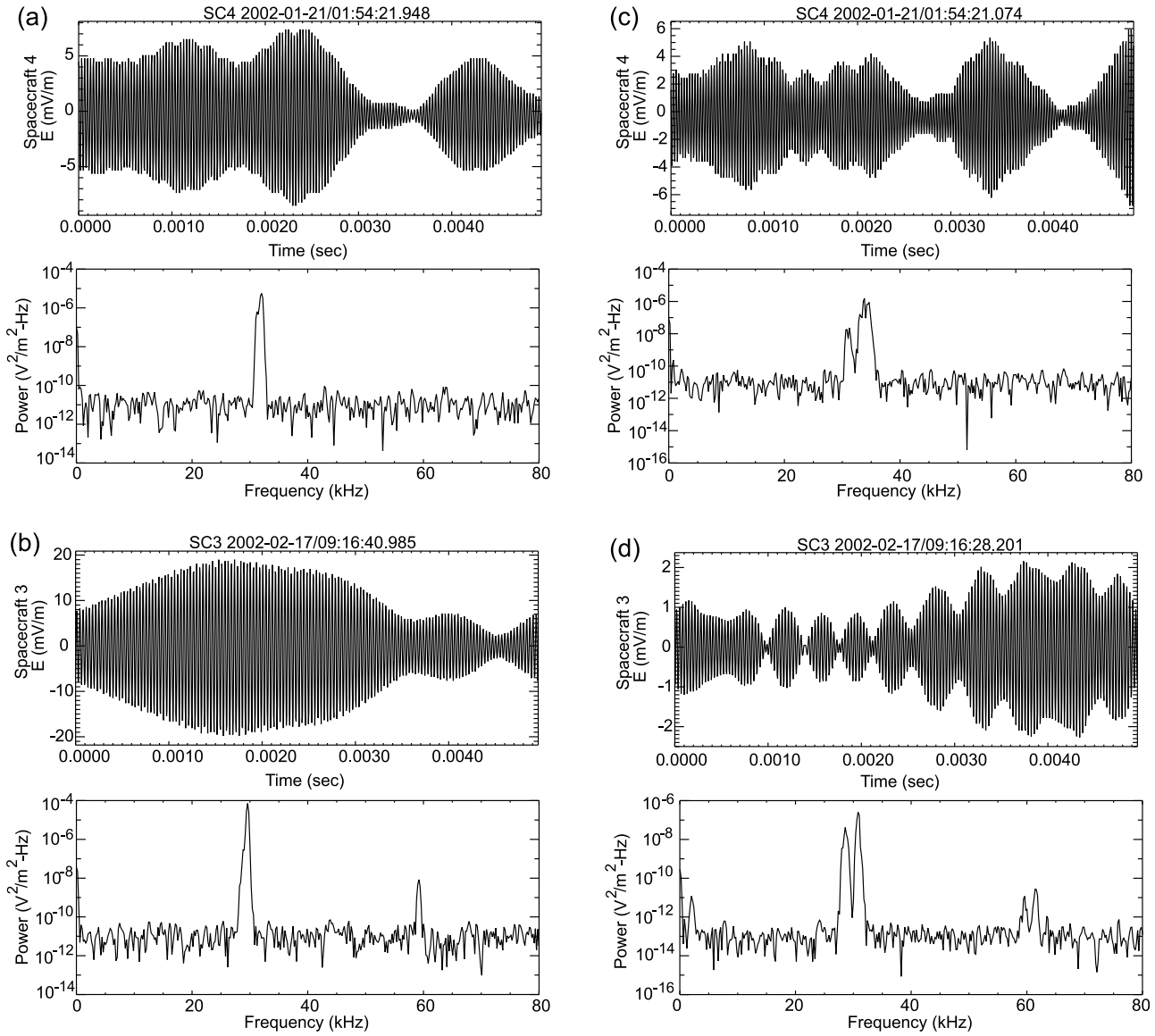

Figure 3. Examples of Cluster WBD waveforms and the corresponding power spectra with (a) peaks near f_{pe}, (b) peaks near f_{pe} and $2f_{pe}$, (c) double peaks near f_{pe}, and (d) double peaks near f_{pe} along with a low frequency peak that could represent ion acoustic waves.

given priority over the harmonic category for two reasons. The first reason is that one of the main goals of this study is to assess the electric field amplitude thresholds for the interaction in equation (1). The second reason is that although double-peaked spectra can exhibit harmonics, many of these harmonics may be instrumental, as we will explore in Section 4.

[20] Figure 4 shows the percentages of the four different types of power spectra illustrated in Figure 3 for (a) amplitudes between 0.1 and 22.0 mV/m and (b) amplitudes greater than 22.0 mV/m on 17 February 2002 and 21 January 2002. These amplitudes have been corrected for the spin modulation of the spacecraft. The amplitude ranges used in Figure 4 were selected because there appeared to be a division in the type of wave behavior observed for amplitudes above and below 22 mV/m, which will be discussed in more detail in Section 5. Applying the spin modulation amplitude correction did not appear to have a significant effect on the overall distribution of the different types of power spectra. The main effect of applying the spin modulation correction was that the amplitude division in the types of power spectra found increased from about 14.0 mV/m to 22.0 mV/m. After the amplitude correction was applied, the percentages of each type of power spectra found in the lower amplitude range on 17 February 2002 changed by less than 1% because of the rejection of waveforms recorded at angles close to 90°, where the spin correction factor becomes very large. On 21 January 2002, the percentages of each type of power spectra found in the lower amplitude range changed by a maximum of about 3%. Applying the spin correction had a slightly stronger effect on the percentages of each type of spectra found in the higher amplitude range for both days due to the combined effects of the rejection of waveforms recorded close to 90°,

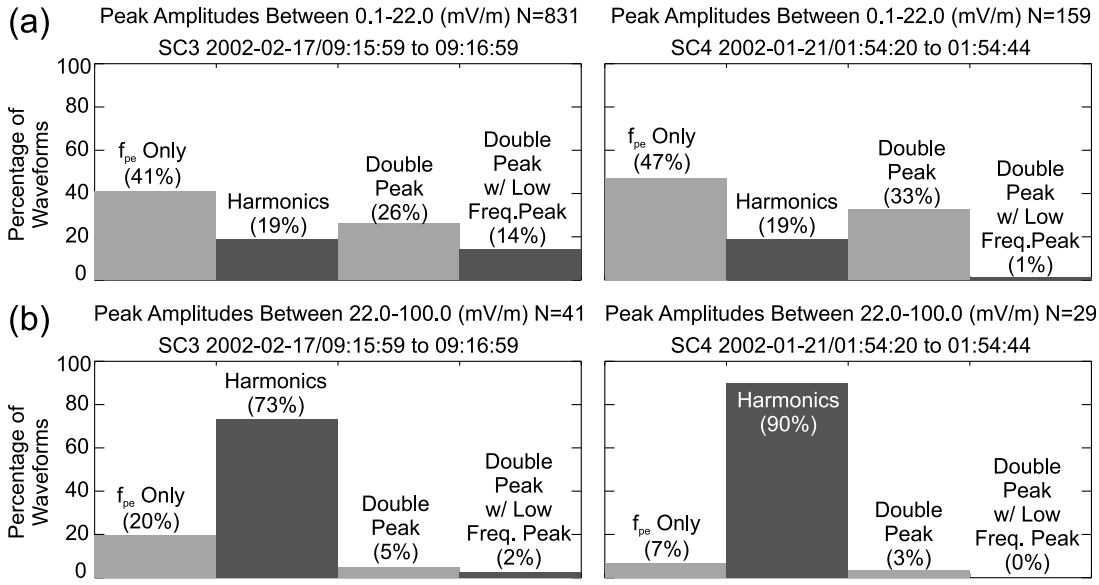

Figure 4. Histograms of the power spectra characteristics on 17 February 2002 and 21 January 2002 for (a) waveforms in the amplitude range 0.1 to 22.0 mV/m, and (b) amplitudes greater than 22.0 mV/m.

waveforms being moved from the lower to the upper amplitude range, and the smaller numbers of waveforms in the higher amplitude range. Overall, on 17 February 2002, only about 14% of the waveforms in the four categories were rejected because they were recorded at antenna spin angles close to 90°. On 21 January 2002, only about 12% of the waveforms were rejected.

[21] The maximum amplitude range of the WBD Plasma Wave Receiver and rejection of clipped waveforms also does not appear to have a significant influence on the statistics, as indicated by a detailed examination of the behavior of the automatic gain control on 17 February 2002 [*Sigsbee et al.*, 2004b]. During the ~1 minute interval of data from spacecraft 3 on 17 February 2002 examined in this paper, 1526 waveforms were recorded and 153 waveforms were rejected due to clipping. Only 13 of these waveforms were recorded in the 0 dB gain state and were definitely outside of the receiver's range. The other clipped waveforms were recorded in gain states with higher amplifications and lower maximum amplitudes, so they may not necessarily have had amplitudes outside the maximum range of the instrument. Many of these clipped waveforms are not completely saturated and only have a few points exceeding the range for the gain setting in which they were recorded, suggesting that their amplitudes are generally within the maximum range of the instrument. During the same time interval on 17 February 2002, the WBD Plasma Wave Receiver on spacecraft 4 was manually set to the 0 dB gain state, permitting observations to be made up to the maximum level of the instrument throughout the entire time period. Only 18 waveforms were clipped on spacecraft 4 during this time period. Because of the bursty nature of foreshock waves, more waveforms were rejected because their amplitudes were below the digitization threshold at which a clear signal can be identified. A similar situation was found during the time interval we examined on 21 January 2002.

[22] The results shown in Figure 4 are similar for both time periods. The largest amplitude waves observed (22.0 mV/m to 100.0 mV/m), generally had power spectra with peaks only at f_{pe} or power spectra with peaks at both f_{pe} and $2f_{pe}$. This is consistent with the idea that the $2f_{pe}$ radio source is located near the foreshock edge, where large amplitude waves are expected. However, as we will discuss shortly, most of the harmonics observed by Cluster may have been caused by instrumental effects. Very few waveforms in this amplitude range had power spectra with double peaks or double peaks and ion acoustic waves. On 21 January 2002, none of the spectra in the 22.0 mV/m to 100.0 mV/m amplitude range fell into the double peak with ion acoustic waves category.

[23] For smaller amplitude waves (0.1 mV/m to 22.0 mV/m), the results were distinctly different from the results for the higher amplitude waves. Figure 4 shows that for 0.1 to 22.0 mV/m, most power spectra fell into the f_{pe}-only category, followed closely by power spectra with double peaks near the local plasma frequency. The results in the 0.1 to 22.0 mV/m amplitude range were similar for both time periods except that the double peak with ion acoustic waves category accounted for only 1% of the spectra on 21 January 2002, which is significantly lower than on 17 February 2002. It is interesting to note that over the entire amplitude range considered, only about 39% of all the spectra on 17 February 2002 had double peaks or double peaks with ion acoustic waves. Over the entire amplitude range considered, only 29% of the spectra on 21 January 2002 had double peaks or double peaks with ion acoustic waves.

4. Harmonic Generation

[24] It is not entirely clear that the harmonics observed in the Cluster WBD receiver data set are produced by the coalescence of the beam-driven and backscattered Langmuir

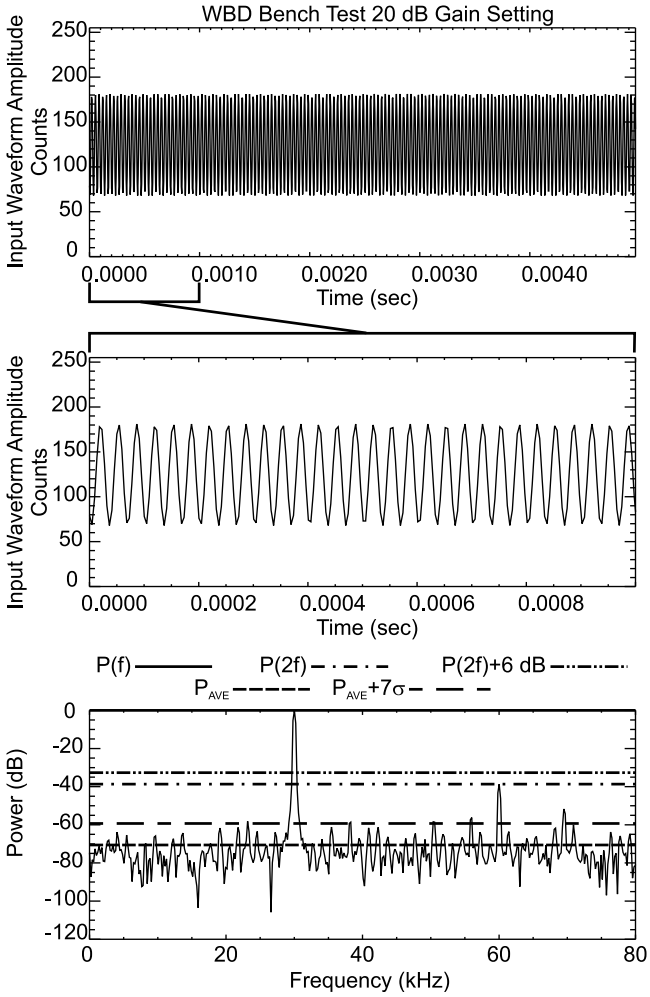

Figure 5. Example waveform and power spectrum from a bench test of the WBD receiver for the 77 kHz mode, the 20 dB gain state, and a 30 kHz input sine wave. The top panel shows the full 1090-point waveform in counts (0–255). The center panel shows an expanded view of 1 millisecond of the waveform. The bottom panel shows the power spectrum of the full 1090-point waveform. Dashed and dotted lines marking the various thresholds used to identify peaks in comparisons with flight data have been marked on the spectra.

waves described in equation (2) because the harmonics are often very weak compared to the fundamental. Following the example of *Cairns* [1986] and *Walker et al.* [2002], we performed a number of tests to determine whether the harmonics observed by Cluster are natural or instrumental.

[25] Bench tests were performed using the spare flight models of the WBD Plasma Wave Receiver and the Ground Support Equipment (GSE) setup for Cluster at the University of Iowa to determine possible instrumental sources of harmonics and the relative amplitudes of these instrumental harmonics to the fundamental. These tests were performed for an input frequency of 30 kHz using the WBD Plasma Wave Receiver's 77 kHz bandwidth mode, which is the mode generally used to study Langmuir waves in the Earth's foreshock. We selected an input frequency of 30 kHz for the bench tests because it was close to the plasma frequency during the two foreshock cases examined in this paper. The bench tests were conducted in the manual gain mode for the gain states used most often in the foreshock, 0 to 35 dB. A function generator with an amplitude range of 0 to 5 V capable of generating sine waves at frequencies of ~30 kHz was used to provide the input signals for the spare WBD Plasma Wave Receiver during the bench tests. To insure that the function generator was producing a clean sine wave at a single frequency, without harmonics, the output of the function generator was examined using a signal analyzer. The behavior of the function generator did not appear to be a significant source of harmonics in our tests. Attenuators were used to bring the input signal from the function generator into the range of the WBD Plasma Wave Receiver for each gain state tested, while using the full voltage range available. Using the GSE setup, the results of the tests were saved to binary data files in the same format as the actual WBD Plasma Wave Receiver frames on board the spacecraft.

[26] Figure 5 shows an example waveform and power spectrum from a bench test of the WBD receiver electronics in the 77 kHz mode and the 20 dB gain setting for an input sine wave with a frequency of 30 kHz. The top panel of Figure 5 shows the full 1090 point waveform with the amplitude given in counts (0–255) centered around the baseline value of approximately 127.5 counts. The second panel of Figure 5 shows an expanded view of the first millisecond of this waveform. The third panel of Figure 5 shows the power spectrum of the full 1090 point waveform. The power spectra of the bench test waveform data were computed using a 1090 point FFT with a Hanning window so that we could characterize instrumental harmonic levels and compare them to harmonics observed in the foreshock.

[27] We found that simply locating the maximum power in a window around the expected harmonic was not a reliable method of harmonic identification due to the variable power spectra background noise levels in both the bench test data and foreshock data. In our bench test data analysis, we examined the background fluctuation levels in the bench test power spectra between 40 and 50 kHz, as no peaks due to instrumental effects were expected in this frequency range. The average background fluctuation level for the bench test waveform shown in Figure 5 has been marked on the spectra with a dashed line. We found that using a threshold of 7 times the standard deviation σ of the background power level was necessary to exclude most random power fluctuations and to help our computer program automatically identify peaks in the power spectra near the expected harmonic at 60 kHz with a reasonable accuracy. The 7σ threshold used to identify peaks has been marked in Figure 5. This approach greatly reduced the number of false positives during the automatic search of the bench test power spectra for harmonics.

[28] When the bench test power near 60 kHz was compared to the background fluctuation levels using the above condition, we found that an instrumental peak near the second harmonic of the input frequency begins to appear when the waveform amplitude reaches about 140 counts, or 20 dB of the 48 dB amplitude range that can be measured for each gain setting. When the values of the bench test power were placed into relative units of dB, we found that for much of the amplitude range in the 0–35 dB gain set-

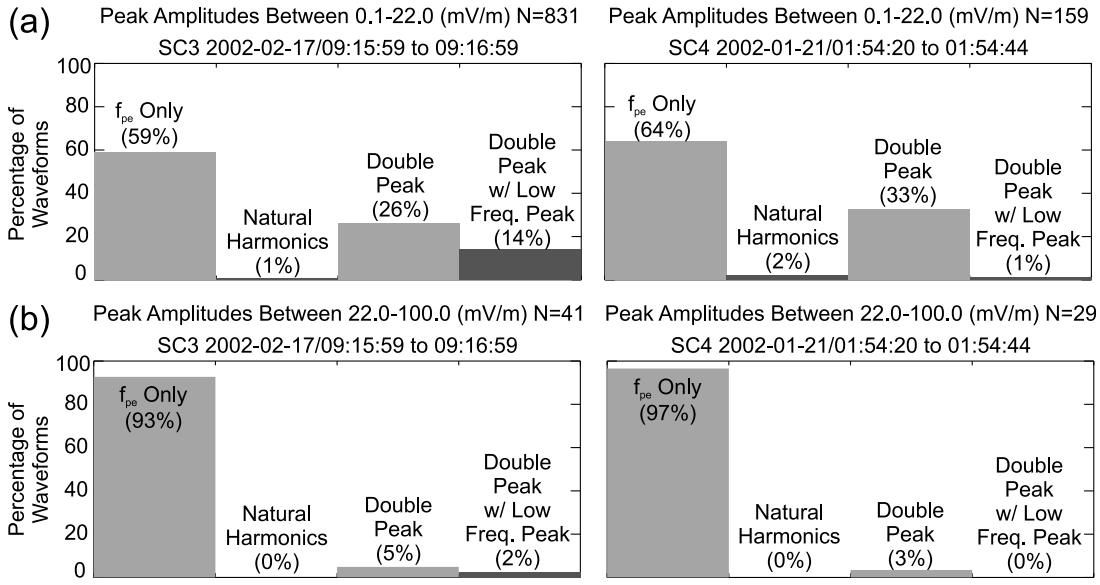

Figure 6. Histograms of the power spectra characteristics on 17 February 2002 and 21 January 2002 for (a) waveforms in the amplitude range 0.1 to 22.0 mV/m, and (b) amplitudes greater than 22.0 mV/m after spectra with instrumental harmonics have been reclassified into the f_{pe}-only category.

tings, the second harmonic produced by the WBD receiver amplifier response is typically about 40 dB down in strength from the fundamental. The power level at the second harmonic in Figure 5 has been marked with a dashed and dotted line and is approximately 40 dB down from the power at the input frequency. In other words, the power at the instrumental second harmonic produced by the WBD receiver amplifiers is a factor of 10^{-4} times weaker than the power at the input frequency. However, when the waveform peak amplitudes reach values close to the maximum levels of 0 and 255 counts, the difference between the power at the second harmonic and the fundamental can be smaller. We suspect that this response is typical of the amplifiers generally used in spaceflight applications and is not unique to the amplifiers on board the Cluster WBD Plasma Wave Receiver.

[29] We then compared the harmonic power levels observed in the foreshock to the bench test results. When analyzing the foreshock data, we searched an 8 kHz window around the expected harmonic frequency to determine the actual location of the harmonic peak. As in the bench tests, peaks near $2f_{pe}$ in the waveform power spectra were only considered if they were more than 7 times the standard deviation σ above the average background power level for that waveform. This was done for consistency with the bench tests and to minimize the number of spectra in the f_{pe} only, double peak, and double peak with ion acoustic waves categories that were flagged as having harmonics by the computer program even though harmonics did not appear to be present during visual inspection of the spectra. Once peaks near $2f_{pe}$ were identified in the foreshock power spectra, we compared the power level near $2f_{pe}$ to the instrumental harmonic levels in bench test waveforms that had the same peak amplitude in counts for the same WBD receiver gain setting used in the foreshock. The bench test harmonic levels used for this comparison were determined by averaging the values of the bench test spectra at the instrumental harmonic peak over all of the bench test waveforms for the same gain setting with the same maximum count values between 0 and 255. Peaks in the power spectra near $2f_{pe}$ were considered to be naturally produced and not instrumental if they were more than 6 dB above the instrumental levels for the same gain setting and same maximum waveform amplitude in counts. In other words, we required that the power near $2f_{pe}$ be greater than the power at the instrumental second harmonic produced by the WBD receiver amplifiers by a factor of 4. The 6 dB threshold used to determine whether harmonics were instrumental or natural has been marked in Figure 5.

[30] Based upon the results of our bench tests, a significant portion of the harmonics observed by the Cluster WBD receiver in the Earth's foreshock may be caused by instrumental effects in the receiver amplifiers. Figure 6 shows the distribution of the four types of spectra we considered after harmonics below the instrumental levels were removed and reclassified into the f_{pe}-only category. For the time period studied on 17 February 2002, there were 156 waveforms with amplitudes between 0.1 and 22 mV/m in the f_{pe} and harmonics category. Only six of these waveforms, or 1% of all waveforms during this time interval, had harmonics more than 6 dB above the instrumental level. For waveforms with amplitudes between 22 and 100 mV/m, there were 30 waveforms in the f_{pe} and harmonics category, but none of them had harmonics more than 6 dB above the instrumental level. A similar result was obtained for 21 January 2002. For amplitudes between 0.1 and 22 mV/m, there were 30 waveforms in the f_{pe} and harmonics category. Only 3 waveforms, or 2% of all waveforms during this time interval, had harmonics more than 6 dB above the instrumental level. There were 26 waveforms with amplitudes between 22 and 100 mV/m in the f_{pe} and harmonics category, but none of these waveforms had harmonic amplitudes at least 6 dB above the instrumental level.

Table 1. Possible Harmonic Observations $0.1 < E < 22$ mV/m on 17 February 2002[a]

Category	N	Harmonic above Instrumental Level	Harmonic f off by More than 1 kHz	Total Noninstrumental Harmonics
f_{pe} and $2f_{pe}$	156	6 (1%)	12 (1%)	17 (2%)
Double peak	217	27 (3%)	29 (4%)	42 (5%)
Double peak with ion acoustic wave	118	2 (less than 1%)	28 (3%)	29 (4%)

[a]Percentages based upon $N = 831$ waveforms.

[31] Although the bench tests suggest that most of the observed harmonics are instrumental, our simple screening of the data based upon the bench test levels may be eliminating some waveforms with weak, natural harmonics. We could therefore be underestimating the percentage of waveforms with harmonics in our study. According to *Cairns* [1986], waves at harmonics of the plasma frequency observed by ISEE-1 sometimes exhibited a directional spin modulation pattern. If the harmonics observed by Cluster WBD are instrumental, their amplitudes must depend on the orientation of the antenna in the same manner as the fundamental. If the harmonics are real, the amplitudes could have different spin modulation patterns from the fundamental. When we examined the spin modulation patterns for spacecraft 3 on 17 February 2002 from 09:15:59 to 09:16:59 UT, we found that the power at f_{pe} and the power at $2f_{pe}$ exhibited the same spin modulation pattern. The power observed at both f_{pe} and $2f_{pe}$ can vary by as much as 10 to 20 dB from their maximum to minimum values as the antennas rotate relative to the magnetic field. Both the power at f_{pe} and the power at $2f_{pe}$ had a minimum value at angles near 90°. The maximum power at both f_{pe} and $2f_{pe}$ occurred when the antennas were most closely aligned with the magnetic field (33° and 150°). The peak electric field values in each waveform exhibit a similar spin modulation pattern and the gain state also changes in response to the electric field variations that result from the changing antenna orientation relative to the magnetic field. Higher gain settings (larger amplifications) are generally needed as the antenna angle approaches 90° to compensate for the smaller signals detected. When we examined the spin modulation patterns for Cluster spacecraft 4 on 21 January 2002 from 01:54:20 to 01:54:44 UT, we found a similar result. The maximum power at both f_{pe} and $2f_{pe}$ occurred when the antennas were most closely aligned with the magnetic field (40° and 140°) and the minimum power occurred when the antennas were perpendicular to the magnetic field. A possible explanation for the difference in the result of the spin modulation checks performed on the ISEE-1 and Cluster data is that the ISEE-1 study used spectral density measurements, which can be strongly affected by spatial and temporal averaging.

[32] During our bench tests, the frequency of the second harmonic caused by amplifier distortion was exactly twice the frequency of the input signal. In data from the foreshock, the frequencies of the waves near the second harmonic might not always be exactly twice the frequency of the fundamental if these signals are natural [*Cairns*, 1986; *Lacombe et al.*, 1988; *Kasaba et al.*, 1997]. According to equation (2), the waves at the second harmonic are electromagnetic in nature, which means they could have propagated to the spacecraft from a location where the plasma frequency is slightly higher or lower than the local plasma frequency measured at the spacecraft. Waves propagating to the spacecraft from another region could also be Doppler shifted. To explore this possibility, we searched an 8 kHz window around the expected harmonic frequency to determine the actual location of the harmonic peak in the foreshock data. Only peaks that were more than 7 times the standard deviation above the average background power were considered.

[33] Table 1 shows the numbers of waveforms for the 0.1 to 22.0 mV/m amplitude range on 17 February 2002 classified into the f_{pe} and $2f_{pe}$, double peak, and double peak with ion acoustic waves categories that may have noninstrumental harmonics. The second column of Table 1 shows the number of waveforms originally sorted into these categories. The third column shows the numbers and percentages of waveforms in these categories found to have harmonics above the instrumental level. The percentages given are based upon the total number of waveforms found in the 0.1 to 22.0 mV/m amplitude range during this time interval. For the f_{pe} and $2f_{pe}$ category, the percentage shown in the third column of Table 1 is the same percentage of waveforms shown in Figure 6. For the time period shown in Table 1, several power spectra were found where the harmonic was located more than 1 kHz away from the expected frequency. The largest difference between the expected and measured harmonic frequency was 2.6 kHz. Some spectra had both harmonics above the instrumental level and harmonics whose frequency differed from the expected value by more than 1 kHz. Each waveform with a possible noninstrumental harmonic was counted only once in the total number of possible noninstrumental harmonics shown in the last column of Table 1. As a result, this value is not equal to the sum of the third and fourth columns. Table 2 shows the same information for the 0.1 to 22.0 mV/m amplitude range

Table 2. Possible Harmonic Observations $0.1 < E < 22$ mV/m on 21 January 2002[a]

Category	N	Harmonic above Instrumental Level	Harmonic f off by More than 1 kHz	Total Noninstrumental Harmonics
f_{pe} and $2f_{pe}$	30	3 (2%)	3 (2%)	5 (3%)
Double peak	52	6 (4%)	7 (4%)	11 (7%)
Double peak with ion acoustic wave	2	0	0	0

[a]Percentages based upon $N = 159$ waveforms.

on 21 January 2002. The largest difference between the expected and measured harmonic frequencies for this amplitude range during the time period studied on 21 January 2002 was 3.4 kHz. For the 22.0 to 100 mV/m amplitude range, no possible noninstrumental harmonics were found on 17 February 2002. Only one was found on 21 January 2002. In this case, the frequency difference between the expected and measured harmonic was 1.2 kHz and the harmonic was not above the instrumental level. Visual inspection of the power spectra revealed that the frequency difference between the expected harmonic and the peak identified by the computer program may be due to a slight broadening of the peaks near f_{pe} and $2f_{pe}$ and the difficulties in automatically identifying peaks near f_{pe} and $2f_{pe}$ when they are superimposed upon large background fluctuations. These examples did not appear to be cases of bifurcation of the $2f_{pe}$ emissions [*Lacombe et al.*, 1988; *Kasaba et al.*, 1997]. Even when the observed harmonic frequency differs from the expected frequency, caution must be used in data interpretation.

[34] Waveforms in the double peak and double peak with ion acoustic wave categories can also have harmonics, as shown by Figure 3(d) and the data in Tables 1 and 2. When the data were screened using a computer program that found the maximum power in an 8 kHz window around the expected $2f_{pe}$, we did find a few waveforms in the double peak and double peak with ion acoustic waves categories that had power near $2f_{pe}$ more than 6 dB above the instrumental harmonic levels determined in our bench tests. If we include these waveforms with the waveforms in the f_{pe} and $2f_{pe}$ category that have possible noninstrumental harmonics, we find that about 10%–11% of all waveforms over the entire amplitude range have noninstrumental harmonics.

[35] However, extra caution must be exercised when examining double-peaked spectra for harmonics. Harmonics such as those in Figure 3(d) are highly suspicious, as they exhibit exactly the same double-peaked structure as the fundamental and are relatively weak, which could indicate they are produced in the receiver amplifiers. Comparison with the bench test harmonic levels can eliminate many instrumental harmonics such as the ones in Figure 3(d). Even when the harmonics do not have exactly the same structure as the peaks near f_{pe}, or the harmonic frequencies were not exactly what were expected, these signals may not be natural. When we tested the receiver electronics, we used only sine wave inputs for simplicity, but the amplifiers can behave differently for nonsinusoidal signals or strong signals with beating waveforms at closely spaced frequencies [*Walker et al.*, 2002]. We did not see much evidence in the foreshock data for the types of nonlinear amplifier behavior reported in the bench tests conducted by *Walker et al.* [2002]. However, a few of the double-peaked power spectra did have harmonics with a complicated structure that could indicate the type of nonlinear instrumental behavior reported in their paper. Based upon our analysis and the results of *Walker et al.* [2002], most of the harmonics found in the double peak and double peak with ion acoustic wave categories are probably instrumental. Other types of wave behavior are often observed in the foreshock, such as broadening of power spectral peaks that can result from time-varying wave frequencies. Nonstationary features such as these could also produce a different instrumental response than what was found in our bench tests using sine wave inputs, so extreme caution must also be used in studying harmonics for these types of waveforms. If we exclude the waveforms from the double peak and double peak with ion acoustic waves categories in Tables 1 and 2 due to the suspicious nature of the harmonics accompanying these waveforms, we find that overall, only about 2%–3% of waveforms during the two time periods we examined have noninstrumental harmonics.

5. Discussion

[36] It appears that most of the harmonics associated with large-amplitude Langmuir waves near the foreshock edge in the Cluster data set were at an amplitude which cannot be distinguished from instrumental effects, but the smaller amplitude waves characterized by double-peaked power spectra may still provide evidence of possible three-wave decay interactions. We varied the amplitude ranges on the histograms in Figure 4 until we discovered that very few power spectra with double peaks or double peaks and ion acoustic waves were observed above an amplitude of 22.0 mV/m. Statistically, during the interval studied on 17 February 2002, there were 20 times more waveforms with amplitudes less than 22.0 mV/m than there were with amplitudes above this value. On 21 January 2002, there were about 5 times more waveforms with amplitudes less than 22.0 mV/m than there were with amplitudes above this value. This means the large amplitude, single peak events represent a small fraction of the total.

[37] One plausible explanation for this threshold effect is that the small group of waveforms with amplitudes above 22.0 mV/m and single-peaked power spectra represent waves which have not yet experienced the decay process. These higher amplitude waves can grow at phase velocities corresponding to higher energy electron beams where Landau damping is decreased. In this scenario, the waveforms with double-peaked power spectra and amplitudes less than 22.0 mV/m represent lower amplitude Langmuir waves and backscattered waves that result after the decay process has occurred. Waveforms with amplitudes less than 22.0 mV/m and single-peaked power spectra have not yet reached the level at which decay occurs. Thus, Figure 4 implies Langmuir wave growth is saturated by some process and that the electrostatic decay threshold in our case studies was usually around a minimum value of 22.0 mV/m, but variations in foreshock conditions sometimes permitted Langmuir waves to grow to larger amplitudes before they eventually succumbed to decay.

5.1. Electrostatic Decay Threshold

[38] To further investigate the causes for the division in the types of Langmuir wave power spectra for amplitudes above and below 22.0 mV/m, we calculated the threshold for electrostatic decay using Cluster data. *Robinson and Cairns* [1995] estimated the maximum Langmuir wave electric fields expected at planetary foreshocks by assuming electrostatic decay saturates beam-driven Langmuir wave

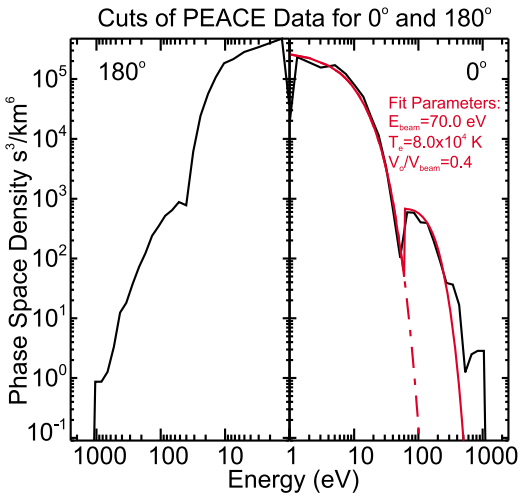

Figure 7. Cluster PEACE electron data for 0° pitch angle (black) showing an electron beam observed by spacecraft 3 on 17 February 2002. The 0° cut of the pitch angle distribution is from the portion of the distribution taken between 09:16:04.109–09:16:04.226 UT and the 180° cut is from the portion of the distribution taken between 09:16:06.112–09:16:06.229 UT. The red line shows a fit to the data of a Maxwellian core distribution plus a half-Maxwellian beam distribution with a center energy of 70 eV.

growth. The random-phase decay has an electric field threshold,

$$E_{L0}^2 = \frac{3}{2\pi\varepsilon_O}\left(1+3\frac{T_i}{T_e}\right)^{-3/2}\sqrt{\frac{M_i}{m_e}}\frac{\gamma_{L'}}{\omega_p}\frac{\Delta\nu}{\nu_b}\frac{V_e}{\nu_b}n_e k_B T_e, \qquad (4)$$

where $\gamma_{L'}$ is the linear damping rate of the product L' wave, ν_b is the electron beam speed, $\Delta\nu$ is the beam's effective thermal spread, and V_e is the electron thermal speed. The threshold depends upon the position in the foreshock due to the electron distribution variation with distance from the foreshock boundary. Using experimental profiles for the solar wind density and temperature dependence on distance from the Sun, *Robinson and Cairns* [1995] estimated E_{L0} ~20 mV/m at 1 AU. *Cairns et al.* [1998] found the threshold was E_{L0} ~2.2 mV/m for typical values near the edge of the Earth's foreshock.

[39] Bursty, intermittent electron beams with energies of 100–200 eV were observed in the foreshock by the Cluster PEACE experiment during the time period we studied on 17 February 2002. Figure 7 shows the Cluster PEACE phase space density for 0° and 180° pitch angle (solid black line) from spacecraft 3 between 09:16:04.109 and 09:16:06.229 UT. The data shown in Figure 7 are 2D Pitch Angle Distribution (PAD) data from the PEACE low energy sensor (LEEA). A fit to the sum of a background Maxwellian distribution with $T = 8.0 \times 10^4$ K and a half-Maxwellian beam distribution centered on 70.0 eV is shown in red for the phase space density at 0°. A phase space weighted average of the energies in the beam at 0° for phase space densities above 1.0 s^3/km^6, yields a beam energy of 115 eV and speed of ν_b = 6400 km/s. The thermal spread of the electron beam from the fit shown in Figure 7 was $\Delta\nu/\nu_b$ ~0.4. Cluster PEACE electron moments indicate that T_e = 1.5×10^5 K (V_e = 1500 km/s) and n_e ~11 cm^{-3}. This value of the electron density gives f_{pe} ~30 kHz, which agrees with the plasma frequency indicated by the WBD receiver. The Cluster CIS experiment indicated kT_i ~35 eV or T_i ~4.1×10^5 K. Following *Cairns et al.* [1998] and assuming $\gamma_{L'}$ ~$10^{-4}\omega_p$ for the linear damping rate of the backscattered waves, these values give E_{L0} ~4.3 mV/m.

[40] The threshold of 4.3 mV/m calculated above for 17 February 2002 does not agree very well with the 22.0 mV/m threshold suggested by Figure 4, but it is consistent with the value of 2.2 mV/m found by *Cairns et al.* [1998] for typical foreshock parameters. *Robinson et al.* [1993] showed that Langmuir wave electric fields could briefly be driven up to $3E_{L0}$ before nonlinear wave damping saturates linear growth. If this is the case, our threshold estimate increases to $3E_{L0}$ ~13 mV/m, which is reasonably close to the threshold indicated by Figure 4, considering the temporal and spatial variability of foreshock electron beams.

[41] There is some uncertainly in the value of $\gamma_{L'}$ used in the above calculation of the electrostatic decay threshold. In an attempt to improve our calculation of E_{L0}, we calculated the damping rate of the backscattered waves $\gamma_{L'}$ based upon the Cluster PEACE electron data. If we assume the waves are Landau damped [*Melrose*, 1986], and that $\nu_b = \omega/k$, as for beam-driven Langmuir waves, we have

$$\gamma_{L'} = \sqrt{\frac{\pi}{2}}\frac{\nu_b^3}{V_e^3}\omega_p \exp\left(-\frac{\nu_b^3}{2V_e^2}\right) \qquad (5)$$

for a Maxwellian electron distribution. Using the same electron parameters as before, we have ν_b/V_e = 4.2, which gives $\gamma_{L'}$ ~$0.01\omega_p$ for the damping rate of the backscattered L' waves. With the plasma parameters used previously, this damping rate gives E_{L0} = 42.6 mV/m, which is higher than the results shown in Figure 4 would suggest. To place the above calculations in context, using the same electron and ion densities and temperatures as above, and increasing the beam energy to 138 eV (ν_b = 6900 km/s, ν_b/V_e = 4.6) would produce a damping rate of $\gamma_{L'}$ ~$2.9 \times 10^{-3}\omega_p$ and E_{L0} = 21.8 mV/m. Beams with speeds of about 7000 km/s have been observed in the foreshock [*Fitzenreiter et al.*, 1984], so these values are not unreasonable. These two estimates of the growth rate give thresholds for electrostatic decay that bracket the observed division in the types of power spectra observed, suggesting that our observations are due to electrostatic decay, but the theory needs further development.

[42] Although a Maxwellian beam is often assumed in calculations of the Landau damping rate, this may not be entirely appropriate for the bump-on-tail electron distributions that arise due to time-of-flight effects in the foreshock. A more general way to determine the Landau damping rate is to examine the dispersion relation for electron plasma oscillations obtained from the Vlasov equation [*Chen*, 1984]

$$\omega^2\left(1 - i\pi\frac{\omega_p^2}{k^2}\left[\frac{\partial f}{\partial \nu}\right]_{\nu=\nu_\varphi}\right) = \omega_p^2, \qquad (6)$$

where k is the wave number and f is the one-dimensional, or reduced distribution function for the electrons, normalized by a factor of $1/n_e$. The damping rate is given by the

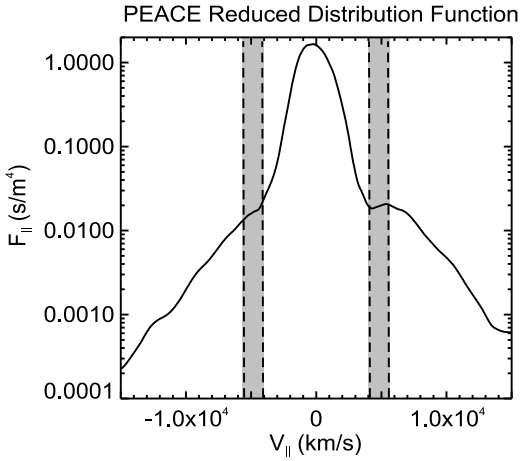

Figure 8. Reduced electron distribution function determined from Cluster PEACE data from spacecraft 3 for the same time period (09:16:04.109 to 09:16:06.229 UT) shown in Figure 7.

imaginary part of ω from equation (6), which depends on the slope of the reduced distribution function, $\partial f/\partial v$ evaluated at the phase velocity, v_φ. Figure 8 shows a reduced distribution function for the same electron beam as in Figure 7. The reduced distribution function was constructed from the 2D PAD LEEA data (CPPADL) taken between 09:16:04.109 and 09:16:06.229 UT after recomputing the pitch angles using high-resolution FGM data and correcting the energy levels for the spacecraft potential. The shaded region on the right-hand side ($V_\parallel > 0$) of Figure 8 indicates where $\partial f/\partial v$ is positive in the electron beam, leading to the growth of beam-driven Langmuir waves. For this electron beam, determining $\partial f/\partial v$ in the positive slope region of the beam yields Langmuir wave growth rates of $\gamma_L \sim 0.001\omega_p$ to $0.01\omega_p$, with an average growth rate of $\gamma_L \sim 0.008\omega_p$. The shaded region on the left-hand side ($V_\parallel < 0$) of Figure 8 indicates a "shoulder" in the reduced distribution function that most likely arises due to the interaction of backscattered Langmuir waves with foreshock electrons. This feature is located at approximately the same velocities as the electron beam on the right-hand side of Figure 8. In the shoulder region, $\partial f/\partial v$ is negative, leading to damping of the backscattered Langmuir waves. Setting ω/k to the average velocity in the shoulder and determining $\partial f/\partial v$ in the shaded region gives damping rates between $\gamma_{L'} \sim 0.008\omega_p$ to $0.02\omega_p$, with an average damping rate of $\gamma_{L'} \sim 0.01\omega_p$ for the backscattered Langmuir waves. For the average damping rate $\gamma_{L'} \sim 0.01\omega_p$, we have E_{L0} = 42.6 mV/m. For the range of damping rates $\gamma_{L'} \sim 0.008\omega_p$ to $0.02\omega_p$, we have E_{L0} = 38.1 mV/m to 60.2 mV/m. These values are consistent with the growth rates estimated using the Landau damping rate for a Maxwellian distribution given in equation (4). These values of E_{L0} are about a factor of 2–3 higher than the 22.0 mV/m threshold indicated by the majority of the waveforms included in Figures 4 and 6. However, the maximum estimate of E_{L0} given above is quite close to the maximum amplitude of 69.7 mV/m observed during the time interval studied on 17 February 2002, consistent with the idea that decay processes can limit wave growth.

[43] The electron beam speeds in the foreshock are highly variable with time and decrease with increasing distance away from the foreshock boundary [*Fitzenreiter et al.*, 1990]. Wind spacecraft data have shown that the stability of foreshock electrons varies with time and unstable bumps can be found in reduced distribution functions from close to the thermal core out to the tail of the distribution at energies approaching 1 keV [*Fitzenreiter et al.*, 1996]. Because of the temporal and spatial variability in the energy and stability of the electron reduced distribution functions, we would expect to have a range of different beam speeds and thresholds for electrostatic decay during the time periods studied. Unfortunately, the time resolution of the Cluster PEACE investigation limits the accuracy of our calculations. The time resolution of PEACE is superior to that of electron measurements made on board earlier spacecraft used to study foreshock waves, such as ISEE, which required 24 s to obtain a complete distribution. However, PEACE still requires a spin period or 4 s to obtain a complete, 3D angular electron distribution over the full energy range of the instrument [*Johnstone et al.*, 1997]. Only partial electron distributions can be obtained over shorter time intervals. In the PEACE PAD data set, part of the 2D pitch angle distribution for a given sensor (HEEA or LEEA) is collected in a single sweep (~125 ms), and the remainder of the distribution is taken half a spin or 2 s later. Thus, the data shown in Figures 7 and 8 represent the 2D electron distribution at approximately 2 s resolution. For a plasma frequency of 30 kHz, the beam-driven Langmuir wave growth rates calculated using equation (6) correspond to time scales between 0.5 and 5 ms. The WBD waveforms in Figure 3 show that foreshock Langmuir wave amplitudes actually do vary on these time scales. We can expect that the electron distributions in the foreshock will also vary on time scales of a few milliseconds in response to the growth and decay of Langmuir waves. Measurements of the full electron distributions are not available on these time scales.

[44] The reduced electron distribution function shown in Figure 8 therefore represents a spatial and temporal average of the electron distribution due to the time required to obtain the full distribution and the motion of the spacecraft during the measurements. This could explain why our best estimates of the electrostatic decay threshold are about a factor of 2–3 times higher than the average threshold indicated by the Langmuir wave spectra. If a decay process is limiting Langmuir wave growth in the foreshock, the variability in beam energies and damping rates can also explain why we occasionally observe spectra with single peaks for waveforms with amplitudes above the 22.0 mV/m decay threshold indicated by the data in Figures 4 and 6. Large amplitude waves generated with smaller k and longer wavelengths by the most energetic electron beams near the foreshock boundary will experience lower damping rates than less intense waves, as indicated by the smaller slope of the reduced distribution function in Figure 8 at high parallel velocities. The lower damping rate may permit waves generated by higher energy beams to exist for longer time periods before being damped away or undergoing decay.

[45] Another possible explanation for the large amplitude waves with single peaks is that the frequency splitting between the backscattered and beam-driven wave is less

than the minimum of ~400 Hz that can be measured with our 1090-point FFT. For the decay interaction shown in equation (1), the frequency separation between the two peaks in the power spectra comes from the relative Doppler shift between the backscattered wave and the forward propagating beam-driven wave due to the solar wind motion [e.g., *Soucek et al.*, 2005],

$$\omega' = \omega - 2\mathbf{k} \cdot \mathbf{V_{sw}}, \tag{7}$$

where $\mathbf{k}$ is the wave vector and $\mathbf{V_{sw}}$ is the solar wind velocity. Note that for a single wave, the solar wind motion would result in a Doppler shift of only $\mathbf{k}\cdot\mathbf{V_{sw}}$. The factor of 2 in equation (7) arises because we are calculating the difference in frequency between two oppositely propagating waves. For V_{sw} = 420 km/s, assuming $\mathbf{k}$ is parallel to $\mathbf{V_{sw}}$ for the beam-driven wave and antiparallel to $\mathbf{V_{sw}}$ for the backscattered wave, an 11 keV beam would be necessary for the separation between the two peaks to be on the edge of our 1090-point FFT's resolution. If the angle between $\mathbf{k}$ and $\mathbf{V_{sw}}$ was 50°, a beam of about 4.5 keV would be necessary. These energies are above the energy of the beam we observed on 17 February 2001 by more than a factor of 10, so it appears unlikely that the splitting was less than the resolution of our FFT.

[46] Recently, modeling and mutual impedance tests of the Cluster antennas have indicated that under certain conditions, the effective length of the antennas may be shorter than their actual physical length [*Béghin et al.*, 2005]. The results of these tests indicate that we may still be underestimating the actual waveform amplitudes, even when we correct for spin modulation. When the antenna response and time resolution of the electron measurements are considered, our results appear to be reasonably consistent with electrostatic decay. However, it is possible that some of the double-peaked power spectra observed by Cluster are not produced by the electrostatic decay described in equation (1). For example, theoretical work and Cluster observations have indicated that foreshock Langmuir waves could instead decay into electron sound waves and ion sound waves. *Soucek et al.* [2005] found the threshold for this process was between a few mV/m to about 20 mV/m for most of the waveforms studied. This is within the range of electric field amplitudes for our two case studies.

[47] Although the amplitude division in the type of power spectra observed appears to be consistent with a decay process, evidence for the ion acoustic waves involved in the electrostatic decay interaction was not found as often as expected. One possible reason why the ion acoustic waves required for three-wave interactions are not observed often is that the ion acoustic waves are weak, strongly damped, and rapidly fall below the instrument's amplitude threshold. Another possible explanation for the lack of double-peaked power spectra with ion acoustic waves is that the frequencies of the ion acoustic waves fall below the 750 Hz lower cutoff of the receiver. For the decay interaction, the frequency of the ion acoustic wave should be related to the Doppler shift between the beam-driven and backscattered waves. For f_{pe} = 30 kHz and V_{SW} = 420 km/s, if the angle between $\mathbf{k}$ and $\mathbf{V_{sw}}$ is 50 degrees, beam speeds greater than 22,000 km/s (1.3 keV) would be needed in order for the frequency of the ion acoustic waves to fall below the receiver cutoff. For f_{pe} = 30 kHz and V_{SW} = 420 km/s, if $\mathbf{k}$ is parallel to $\mathbf{V_{sw}}$, beam speeds greater than 30,000 km/s (3.2 keV) would be needed. However, in some double-peaked power spectra, such as the example in Figure 3(c), the separation between the L and L' wave peaks is wide enough that we should be able to resolve a peak for the ion acoustic wave, but we do not have a clear low-frequency peak. Ion acoustic waves may be products of electrostatic decay or they may be generated through instabilities associated with heat conduction in the solar wind [*Forslund*, 1970; *Gurnett and Anderson*, 1977]. As shown in equation (1), preexisting ion acoustic waves could also undergo a coalescence with Langmuir waves to generate the backscattered waves. Following the example of *Gurnett and Anderson* [1977], we estimated the range of Doppler-shifted ion acoustic wave frequencies that would be possible based upon the plasma parameters used in our calculations of E_{L0}. We found that the Doppler-shifted frequencies of ion acoustic waves generated by processes other than electrostatic decay should theoretically be within the range of the WBD receiver for a broad range of propagation angles relative to the solar wind velocity. Foreshock electron distributions, such as the one in Figure 7, often show evidence for a backscattered L' wave population. If the power spectra and electron distributions show evidence of a backscattered wave population, but ion acoustic waves are not present, some other process may be at work.

[48] The double-peaked power spectra in these cases may instead be produced by the reflection of Langmuir waves from inhomogeneities in the solar wind plasma [e.g., *Kellogg et al.*, 1999b]. When Langmuir waves encounter regions where the wave frequency is less than the local plasma frequency, they can be reflected, mode converted to transverse electromagnetic waves, and trapped in density wells [*Willes and Cairns*, 2001]. Reflection by density gradients produces backscattered waves and could explain the low percentage of double-peaked power spectra with ion acoustic waves found in the Cluster data. Wave scattering off thermal ions [*Muschietti and Dum*, 1991, *Muschietti et al.*, 1996, *Mitchell et al.*, 2003] could also have produced some double-peaked power spectra and explain the waves at $2f_{pe}$ [*Yoon et al.*, 1994]. However, theoretical considerations indicate that this process is not significant in the Earth's foreshock, except for very intense wave packets [*Cairns*, 2000]. The waveforms associated with power spectra of the types shown in Figure 3(c) and 3(d) sometimes show evidence for beating between the different wave populations, in the form of phase changes near the zero crossings of the waveform electric field. The reflection of Langmuir waves by plasma inhomogeneities provides an alternate explanation to electrostatic decay for beat-like waveforms with irregular envelopes [*Willes and Cairns*, 2001]. Recent work based upon observations from the STEREO S/WAVES instrument in the solar wind has suggested that the Langmuir wave envelopes and power spectra featuring double peaks and side lobes can be explained by Langmuir wave eigenmodes trapped in parabolic density wells [*Ergun et al.*, 2008]. While wave reflection, mode conversion, and eigenmode structures could also play a role in the foreshock, our data and decay threshold calculations suggest that Langmuir wave decay still may be an important process during the time periods studied.

5.2. Modulational Instability

[49] Many authors have discussed the modulational instability as another possible mechanism for the saturation of Langmuir waves in the Earth's foreshock, as well as in the source regions of type III solar radio bursts [*Thejappa et al.*, 1999]. The physics of strong turbulence and modulational instabilities, as well as the decay processes important in weak turbulence interactions, can be described using the Zakharov equations [*Zakharov*, 1972]. To determine if decay processes or the modulational instability are allowed for the February 17, 2002 case study, we consider the dimensionless energy density of the pump Langmuir waves [*Robinson*, 1997],

$$W = \frac{\varepsilon_0 E^2}{4 n_e k_B T_e}, \tag{8}$$

where E is the electric field amplitude of the waves. Electrostatic decay processes will dominate over modulational instabilities [*Robinson*, 1997; *Cairns et al.*, 1998] when

$$W < k\lambda_D \left(\frac{m_e}{M_i}\right)^{1/2} \tag{9}$$

$$k\lambda_D > \frac{1}{3}\sqrt{\left(\frac{m_e}{M_i}\right)\left(1 + 3\frac{T_i}{T_e}\right)}. \tag{10}$$

Even for the largest amplitude uncorrected electric fields, E = 36.9 mV/m, that can be observed by the Cluster WBD receiver, we only have $W = 1.3 \times 10^{-4}$ using the same plasma parameters as before. Using the largest spin corrected amplitude found on 17 February 2002, E = 69.7 mV/m, gives $W = 4.7 \times 10^{-4}$. For the calculated Debye length of λ_D = 8.1 m and assuming $\nu_b = \omega/k$, we have $k\lambda_D \sim 0.24$, so that the right-hand side of equation (9) is 5.6×10^{-3}. This is more than a factor of 10 greater than W for even the largest amplitude waves observed during the time interval we considered, which are too small for the modulational instability to occur. For our plasma and beam parameters, equation (9) would hold true until the wave amplitudes reached values well over 200 mV/m. The condition on the wave number given in equation (10) can be rewritten in terms of the electron beam speed and thermal speed so that we have

$$\frac{\nu_b}{V_e} \leq 3\sqrt{\frac{M_i}{m_e\left(1 + 3\frac{T_i}{T_e}\right)}}, \tag{11}$$

which gives the maximum beam speed allowed for electrostatic decay to proceed [*Cairns et al.*, 1998]. For the beam speed and temperatures used in our calculation of the electrostatic decay threshold, the value of the right-hand side of equation (11) is about 42, a factor of 10 larger than the ratio of the electron beam speed and thermal speed, ν_b/V_e = 4.2. This suggests that the beam in our example is well below the maximum beam speed allowed for electrostatic decay. Even if the ion temperature was considerably lower or higher, so that T_i/T_e = 1/3 or T_i/T_e = 5, we would still be well within the regime where electrostatic decay is permitted for our beam parameters and electron temperature. Thus, we conclude that our data are consistent with electrostatic decay and not consistent with the modulational instability. This agrees with past studies [*Cairns et al.*, 1998; *Bale et al.*, 1997; *Kellogg et al.*, 1999a] showing that the Langmuir wave amplitudes in the Earth's foreshock are not sufficient for modulational instabilities and wave collapse.

6. Conclusions

[50] We performed statistical analysis on Langmuir wave power spectra from the Earth's foreshock to determine how often the signatures of three-wave interactions and waves at harmonics of the plasma frequency are observed in the Cluster data set. Power spectra with double peaks near f_{pe} are mainly observed for lower amplitude waves (< 22.0 mV/m), but the ion acoustic waves required for three-wave interactions are not observed very often. Either the ion acoustic waves are weak and strongly damped, or other processes, such as wave reflection and mode conversion, are responsible for some of the double-peaked power spectra. The types of spectra found for waveforms with amplitudes less than 22.0 mV/m and the lack of large numbers of waveforms above 22.0 mV/m may be related to saturation of wave growth by electrostatic decay processes in the foreshock. Theoretical predictions of the decay threshold do not agree well with our experimentally determined threshold, but the predicted values are consistent with the observed range of maximum amplitudes and the idea that Langmuir wave growth is saturated by decay processes. The beam parameters, electric field amplitudes, and wave vectors in the 17 February 2002 case study appear to be well within the regime where decay processes should dominate over modulational instabilities.

[51] We found that many of the largest amplitude waves near the foreshock edge were emissions at f_{pe} and $2f_{pe}$, which initially appeared to be consistent with past studies showing that the most intense $2f_{pe}$ radio emissions occur at the foreshock edge [*Lacombe et al.*, 1988; *Kasaba et al.*, 2000]. However, a significant portion of the harmonics observed by the Cluster were very weak compared to the fundamental and could not be clearly distinguished from harmonics generated by nonlinear instrumental effects. Detailed comparison with the results from bench tests of the Cluster WBD Plasma Wave Receiver indicated that only a few percent of the harmonics observed in the foreshock may be natural. As the types of nonlinear instrumental effects examined in this paper and by *Walker et al.* [2002] are a feature of all amplifier circuits and are not unique to the Cluster WBD Plasma Wave Receiver, future investigators studying harmonic generation in the Earth's foreshock or any other region of space need to compare all observed harmonics to the instrumental levels found during calibration before conducting in-depth studies of possible natural generation processes.

[52] **Acknowledgments.** This work was supported by NASA grant NNX07AI24G. The authors would like to thank Iver Cairns for helpful discussions about the Langmuir wave decay. We would also like to thank Jim Phillips and William Robison for assistance with the WBD bench tests. We

thank the ACE SWEPAM and MAG Instrument Teams and the ACE Science Data Center for providing the ACE data.

[53] Zuyin Pu thanks S. D. Bale and another reviewer for their assistance in evaluating this paper.

References

Bale, S. D., D. Burgess, P. J. Kellogg, K. Goetz, R. L. Howard, and S. J. Monson (1996), Phase coupling in Langmuir wave packets: Possible evidence of three-wave interactions in the upstream solar wind, *Geophys. Res. Lett.*, *23*(1), 109–112.

Bale, S. D., D. Burgess, P. J. Kellogg, K. Goetz, and S. J. Monson (1997), On the amplitude of intense Langmuir waves in the terrestrial electron foreshock, *J. Geophys. Res.*, *102*(A6), 11281–11286.

Bale, S., D. Larson, R. Lin, P. Kellogg, K. Goetz, and S. Monson (2000), On the beam speed and wavenumber of intense electron plasma waves near the foreshock edge, *J. Geophys. Res.*, *105*(A12), 27,353–27,367.

Balogh, A., C. M. Carr, M. H. Acuña, M. W. Dunlop, T. J. Beek, P. Brown, K.-H. Fornaçon, E. Georgescu, K.-H. Glassmeier, J. Harris, G. Musmann, T. Oddy, and K. Schwingenschuh (2001), The Cluster magnetic field investigation: Overview of in-flight performance and initial results, *Ann. Geophys.*, *19*, 1207.

Béghin, C., P. M. E. Décréau, J. Pickett, D. Sundkvist, and B. Lefebvre (2005), Modeling of Cluster's electric antennas in space: Application to plasma diagnostics, *Radio Sci.*, *40*, RS6008, doi:10.1029/2005RS003264.

Bougeret, J.-L., M. K. Kaiser, P. J. Kellogg, R. Manning, K. Goetz, S. J. Monsoon, N. Monge, L. Friel, C. A. Meetre, C. Perche, L. Sitruk, and S. Hoang (1995), Waves: The radio and plasma wave investigation on the Wind spacecraft, *Space Sci. Rev.*, *71*, 231–263.

Cairns, I. H. (1986), New waves at multiples of the plasma frequency upstream of the Earth's bow shock, *J. Geophys. Res.*, *91*(A3), 2975–2988.

Cairns, I. H. (2000), Role of collective effects in dominance of scattering off thermal ions over Langmuir wave decay: Analysis, simulations, and space applications, *Phys. Plasmas*, *7*(12), 4901–4915.

Cairns, I. H., and D. B. Melrose (1985), A theory for the $2f_p$ radiation upstream of the Earth's bow shock, *J. Geophys. Res.*, *90*(A7), 6637–6640.

Cairns, I. H., and P. A. Robinson (1992), Theory for low-frequency modulated Langmuir wave packets, *Geophys. Res. Lett.*, *19*(22), 2187–2190.

Cairns, I. H., P. A. Robinson, R. R. Anderson, and R. J. Strangeway (1997), Foreshock Langmuir waves for unusually constant solar wind conditions: Data and implications for foreshock structure, *J. Geophys. Res.*, *102*(A11), 24,249–24,264.

Cairns, I. H., P. A. Robinson, and N. I. Smith (1998), Arguments against modulational instabilities of Langmuir waves in Earth's foreshock, *J. Geophys. Res.*, *103*(A1), 287–299.

Chen, F. F. (1984), *Introduction to Plasma Physics and Controlled Fusion, Volume 1: Plasma Physics*, Plenum Press, New York.

Ergun, R. E., et al. (2008), Eigenmode structure in solar-wind Langmuir waves, *Phys. Rev. Lett.*, *101*(5), 051101, doi:10.1103/PhysRevLett.101.051101.

Etcheto, J., and M. Faucheux (1984), Detailed study of electron plasma waves upstream of the Earth's bow shock, *J. Geophys. Res.*, *89*(A8), 6631–6653.

Farrell, W. M., M. L. Kaiser, S. D. Bale, M. D. Desch, R. J. Fitzenreiter, K. Goetz, and J.-L. Bougeret (2004), Relativistic cyclotron resonance condition as applied to Type II interplanetary radio emission, *J. Geophys. Res.*, *109*, A02106, doi:10.1029/2003JA009965.

Filbert, P. C., and P. J. Kellogg (1979), Electrostatic noise at the plasma frequency beyond the Earth's bow shock, *J. Geophys. Res.*, *84*(A4), 1369–1381.

Fitzenreiter, R. J., A. J. Klimas, and J. D. Scudder (1984), Detection of bump-on-tail reduced electron velocity distributions at the electron foreshock boundary, *Geophys. Res. Lett.*, *11*(5), 496–499.

Fitzenreiter, R. J., J. D. Scudder, and A. J. Klimas (1990), Three-dimensional analytical model for the spatial variation of the foreshock electron distribution function: Systematics and comparisons with ISEE observations, *J. Geophys. Res.*, *95*(A4), 4155–4173.

Fitzenreiter, R. J., A. F. Viñas, A. J. Klimas, R. P. Lepping, M. L. Kaiser, and T. G. Onsager (1996), Wind observations of the electron foreshock, *Geophys. Res. Lett.*, *23*(10), 1235–1238.

Forslund, D. W. (1970), Instabilities associated with heat conduction in the solar wind and their consequences, *J. Geophys. Res.*, *75*(1), 17–28.

Fredricks, R. W., F. L. Scarf, and L. A. Frank (1971), Nonthermal electrons and high-frequency waves in the upstream solar wind 2. Analysis and interpretation, *J. Geophys. Res.*, *76*(28), 6691–6699.

Fuselier, S. A., D. A. Gurnett, and R. J. Fitzenreiter (1985), The downshift of electron plasma oscillations in the electron foreshock region, *J. Geophys. Res.*, *90*(A5), 3935–3946.

Gurnett, D. A. (1975), The Earth as a radio source: The nonthermal continuum, *J. Geophys. Res.*, *80*(19), 2751–2763.

Gurnett, D. A., and R. R. Anderson (1977), Plasma wave electric fields in the solar wind: Initial results from Helios 1, *J. Geophys. Res.*, *82*(4), 632–650.

Gurnett, D. A., R. L. Huff, and D. L. Kirchner (1997), The wide-band plasma wave investigation, *Space Sci. Rev.*, *79*(1–2), 195–208.

Henri, P., C. Briand, A. Mangeney, S. D. Bale, F. Califano, K. Goetz, and M. Kaiser (2009), Evidence for wave coupling in type III emissions, *J. Geophys. Res.*, *114*, A03103, doi:10.1029/2008JA013738.

Hoang, S., J. Fainberg, J. L. Steinberg, R. G. Stone, and R. H. Zwickl (1981), The 2fp circumterrestrial radio radiation as seen from ISEE 3, *J. Geophys. Res.*, *86*(A6), 4531–4536.

Johnstone, A. D., et al. (1997), PEACE: A plasma electron and current experiment, *Space Sci. Rev.*, *79*(1–2), 351–398.

Kasaba, Y., H. Matsumoto, and R. R. Anderson (1997), Geotail observation of $2f_p$ emission around the terrestrial electron foreshock, *Adv. Space. Res.*, *20* (4/5), 699–702.

Kasaba, Y., H. Matsumoto, Y. Omura, R. R. Anderson, T. Mukai, Y. Saito, T. Yamamoto, and S. Kokubun (2000), Statistical studies of plasma waves and backstreaming electrons in the terrestrial electron foreshock observed by Geotail, *J. Geophys. Res.*, *105*(A1), 79–103.

Kellogg, P. J. (2003), Langmuir waves associated with collisionless shocks; A review, *Planetary and Space Science*, *51*, 681–691.

Kellogg, P. J., S. J. Monson, K. Goetz, R. L. Howard, J. Bougeret, and M. L. Kaiser (1996), Early Wind observations of bow shock and foreshock waves, *Geophys. Res. Lett.*, *23*(10), 1243–1246.

Kellogg, P. J., K. Goetz, S. J. Monson, and S. D. Bale (1999a), A search for Langmuir solitons in the Earth's foreshock, *J. Geophys. Res.*, *104*(A4), 6751–6757.

Kellogg, P. J., K. Goetz, S. J. Monson, and S. D. Bale (1999b), Langmuir waves in a fluctuating solar wind, *J. Geophys. Res.*, *104*(A8), 17,069–17,078.

Lacombe, C., A. Mangeney, C. C. Harvey, and J. D. Scudder (1985), Electron plasma waves upstream of the Earth's bow shock, *J. Geophys. Res.*, *90*(A1), 73–94.

Lacombe, C., C. C. Harvey, S. Hoang, A. Mangeney, J.-L. Steinberg, and D. Burgess (1988), ISEE observations of radiation at twice the solar wind plasma frequency, *Ann. Geophys.*, *6*(1), 113–128.

Leroy, M. M., and A. Mangeney (1984), A theory of energization of solar wind electrons by the Earth's bow shock, *Ann. Geophys.*, *2*(4), 449–456.

Lobzin, V. V., V. V. Krasnoslskikh, S. J. Schwartz, I. Cairns, B. Lefebvre, P. Décréau, and A. Fazakerley (2005), Generation of downshifted oscillations in the electron foreshock: A loss-cone instability, *Geophys. Res. Lett.*, *32*, L18101, doi:10.1029/2005GL023563.

Marsch, E. (1985), Beam-driven electron acoustic waves upstream of the Earth's bow shock, *J. Geophys. Res.*, *90*(A7), 6327–6336.

Melrose, D. B. (1986), *Instabilities in Space and Laboratory Plasmas*, Cambridge University Press, New York.

Mitchell, J. J., I. H. Cairns, and P. A. Robinson (2003), New constraints and energy conversion efficiencies for plasma emission, *Phys. Plasmas*, *10*(8), 3315–3329, doi:10.1063/1.1589491.

Muschietti, L., and C. T. Dum (1991), Nonlinear wave scattering and electron beam relaxation, *Phys. Fluids B*, *3*(8), 1968–1982.

Muschietti, L., I. Roth, and R. E. Ergun (1996), On the formation of wave packets in planetary foreshocks, *J. Geophys. Res.*, *101*(A7), 15,605–15,613.

Reme, H., et al. (2001), First multispacecraft ion measurements in and near the Earth's magnetosphere with the identical Cluster ion spectrometry (CIS) experiment, *Ann. Geophys.*, *19*(10–12), 1303–1354.

Robinson, P. A. (1997), Nonlinear wave collapse and strong turbulence, *Reviews of Modern Physics*, *69*(2), 507–573.

Robinson, P. A., and I. H. Cairns (1995), Maximum Langmuir fields in planetary foreshocks determined from the electrostatic decay threshold, *Geophys. Res. Lett. 22*(19), 2657–2660.

Robinson, P. A., A. J. Willes, and I. H. Cairns (1993), Dynamics of Langmuir and ion sound waves in type III solar radio sources, *Astrophys. J.*, *408*(2), 720–734.

Scarf, F. L., R. W. Fredricks, L. A. Frank, and M. Neugebauer (1971), Nonthermal electrons and high-frequency waves in the upstream solar wind, *J. Geophys. Res.*, *76*(22), 5162–5171.

Sigsbee, K., C. A. Kletzing, D. A. Gurnett, J. S. Pickett, A. Balogh, and E. Lucek (2004a), The dependence of Langmuir wave amplitudes on position in Earth's foreshock, *Geophys. Res. Lett.*, *31*, L07805, doi:10.1029/2004GL019413.

Sigsbee, K., C. A. Kletzing, D. A. Gurnett, J. S. Pickett, A. Balogh, and E. Lucek (2004b), Statistical behavior of foreshock Langmuir waves observed by the Cluster Wideband Data Plasma Wave Receiver, *Ann. Geophys.*, *22*(7), 2337–2344.

Soucek, J., V. Krasnoselskikh, T. Dudok de Wit, J. Pickett, and C. Kletzing (2005), Nonlinear decay of foreshock Langmuir waves in the presence of

plasma inhomogeneities: Theory and Cluster observations, *J. Geophys. Res.*, *110*, A08102, doi:10.1029/2004JA010977.

Thejappa, G., M. L. Goldstein, R. J. MacDowall, K. Papadopoulos, and R. G. Stone (1999), Evidence for Langmuir envelope solitons in solar type III burst source regions, *J. Geophys. Res.*, *104*(A12), 28,279–28,293.

Walker, S. N., M. A. Balikhin, I. Bates, and R. Huff (2002), An investigation into instrumental nonlinear effects, *Adv. Space Res.*, *30*(12), 2815–2820.

Walker, S. N., J. S. Pickett, D. A. Gurnett, and H. Alleyne (2003), High order spectral analysis of electron plasma oscillations in the electron foreshock, *Adv. Space Res.*, *32*(3), 309–314.

Willes, A. J., and I. H. Cairns (2001), Mode conversion and reflection of Langmuir waves in an inhomogeneous solar wind, *Publ. Astron. Soc. Aust.*, *18*(4), 335–360.

Wu, C. S. (1984), A fast Fermi process: Energetic electrons accelerated by a nearly perpendicular bow shock, *J. Geophys. Res.*, *89*(A10), 8857–8862.

Yoon, P. H., C. S. Wu, A. F. Vinas, M. J. Reiner, J. Fainberg, and R. G. Stone (1994), Theory of $2\omega_{pe}$ radiation induced by the bow shock, *J. Geophys. Res.*, *99*(A12), 23,481–23,488.

Zakharov, V. E. (1972), Collapse of Langmuir waves, *Sov. Phys. JETP*, *35*(5), 908–914.

A. N. Fazakerley, Mullard Space Science Laboratory, Dorking, RH5 6NT, UK.

D. A. Gurnett, C. A. Kletzing, J. S. Pickett, and K. Sigsbee, Department of Physics and Astronomy, University of Iowa, Iowa City, IA 52242, USA.

B. Lefebvre and H. Kucharek, University of New Hampshire, Space Science Center, Durham, NH 03824, USA.

E. Lucek and S. J. Schwartz, Space and Atmospheric Physics Group, The Blackett Laboratory, Imperial College, London, SW7 2AZ, UK.